



Spatial and temporal variations of the Kuroshio east of Taiwan, 1982–2005: A numerical study

Yi-Chia Hsin,¹ Chau-Ron Wu,¹ and Ping-Tung Shaw²

Received 4 August 2007; revised 5 November 2007; accepted 28 December 2007; published 3 April 2008.

[1] A $1/8^\circ$ East Asian Marginal Seas model nested to a larger-domain North Pacific Ocean model is implemented over a span of 24 years from 1982 to 2005 to investigate the spatial and temporal variations of the Kuroshio east of Taiwan. Between 22° and 25°N , the mean state and variability of the Kuroshio, such as the two paths observed in the trajectories of surface drifters southeast of Taiwan and the branching of the Kuroshio northeast of Taiwan, are well reproduced by the model. Southeast of Taiwan, the Kuroshio is mostly in the top 300 m in the inshore path but extends to 600 m in the offshore path. Northeast of Taiwan, the Kuroshio follows the shelf edge in the East China Sea but may branch along a path south of the Ryukyu Islands. The latter path often meanders southward, and a significant portion of the Kuroshio transport may be diverted to this path. The Kuroshio extends from the coast to $123\text{--}123.5^\circ\text{E}$ between 22° and 25°N with currents reaching a depth of 1000 m at some latitudes. The Kuroshio transports averaged over five sections east of Taiwan are 28.4 ± 5.0 Sv and 32.7 ± 4.4 Sv with and without the contribution from the countercurrent, respectively.

Citation: Hsin, Y.-C., C.-R. Wu, and P.-T. Shaw (2008), Spatial and temporal variations of the Kuroshio east of Taiwan, 1982–2005: A numerical study, *J. Geophys. Res.*, 113, C04002, doi:10.1029/2007JC004485.

1. Introduction

[2] The Kuroshio is the most important current in the seas east of Taiwan. It originates from the North Equatorial Current that bifurcates between 12° and 15°N in the western equatorial Pacific Ocean [Qu and Lukas, 2003]. The southward branch is the Mindanao Current, and the northward branch becomes the Kuroshio [Nitani, 1972; Qiu and Lukas, 1996; Qu et al., 1998; Centurioni et al., 2004; Yaremchuk and Qu, 2004]. The Kuroshio flows northward along the coasts of Luzon and Taiwan, continues to the shelf edge of the East China Sea, and finally becomes the Kuroshio Extension after departing from Japan [Nitani, 1972]. The Kuroshio transports warm water from the tropical ocean to midlatitudes and is an important source of heat for the atmosphere in the global heat balance [Qu, 2003].

[3] The Kuroshio east of Taiwan has been studied extensively using in situ data from both hydrographic and current meter measurements. On the basis of hydrographic surveys from eight cruises, Chu [1974] found large spatial and temporal flow variability in the Kuroshio east of Taiwan. For example, the distance of the high-velocity core from the coast of Taiwan at 23.75°N ranges from 30 to 120 km with maximum current speeds between 60 and 120 cm/s. Table 1

summarizes the estimates of the Kuroshio transport east of Taiwan in earlier studies. The transport varies between 15 and 44 Sv ($1 \text{ Sv} = 10^6 \text{ m}^3/\text{s}$) with a smaller range of 15–26 Sv in studies after 1990. The large range of transport values may be contributed by the variation of the flow in the Kuroshio but may also be a result of the methods and data used in computation. For example, Nitani [1972] estimated the Kuroshio transport relative to several reference pressure surfaces; the transport relative to the 800 dbar pressure surface is about 80% of the value relative to the 1200 dbar pressure surface.

[4] Recent composite pictures of the velocity field obtained from shipboard acoustic Doppler current profilers (Sb-ADCP) between 1990 and 2001 [Liang et al., 2003] indicated that the Kuroshio is 150–200 km wide and splits into two paths when reaching the Lan-Yu Island (Figure 1c). The two paths join again at 23°N . Afterward, the Kuroshio flows into the East China Sea through the East Taiwan Channel (ETC) between Taiwan and the Ishigakijima (Figure 1c). A mooring array was deployed during the World Ocean Circulation Experiment along an extensively studied section called PCM-1 in ETC between September 1994 and May 1996. The flow direction during this period varies greatly, indicating large meandering of the current [Zhang et al., 2001]. The mean transport obtained is 21.5 ± 2.5 Sv over the 20-month period with a dominant period of 3–4 months (~ 100 d) [Johns et al., 2001; Zhang et al., 2001]. Using the empirical orthogonal function analysis, Zhang et al. [2001] suggested two principal components in the horizontal flow field: meandering of the Kuroshio axis at multiple periods of 100, 40, and 18 d and fluctuation of the transport at 100 d.

¹Department of Earth Sciences, National Taiwan Normal University, Taipei, Taiwan.

²Department of Marine, Earth, and Atmospheric Sciences, North Carolina State University, Raleigh, North Carolina, USA.

Table 1. Mean Kuroshio Transport East of Taiwan in Earlier Observations^a

Publication	Period	Position	Method	Mean Q, Sv
<i>Chu</i> [1970]	Sep 1965–May 1967 (4 cruises)	21.75–23.75°N	geostrophic (RD = 800 dbar)	17.8–20.4
<i>Nitani</i> [1972]	1965–1967 (5 cruises)	~23°N	geostrophic (RD = 1200 dbar)	40
<i>Nitani</i> [1972]	1942–1966 (5 cruises)	25°N	geostrophic (RD = 1200 dbar)	33
<i>Chu</i> [1976]	1974–1975 (6 cruises)	~24°N	geostrophic (RD = 800 dbar)	29.3
<i>Liu</i> [1983]	26–29 Jul 1983 (1 cruise)	24°N	geostrophic	44.2
<i>Liu et al.</i> [1998]	Oct 1990–May 1995 (12 cruises)	ETC (~24.5°N)	adjusted geostrophic and Sb-ADCP	19.7 (0–350 m) 22.6 (0–bottom)
<i>Johns et al.</i> [2001]	19 Sep 1994–May 27 1996	ETC (~24.5°N)	mooring array (3 methods)	21.5 ± 2.5
<i>Hwang and Kao</i> [2002]	Dec 1992–Apr 2000	southeast (~22°N) and northeast (~24.5°N) of Taiwan	TOPEX/Poseidon altimeter	19±6 (northeast) 26 ± 5 (southeast)
<i>Gilson and Roemmich</i> [2002]	1993–2001 (34 cruises)	southeast of Taiwan (0–800 m)	geostrophic (RD = 800 m)	22.0 ± 1.5
<i>Yang and Liu</i> [2003]	Nov 1992–Jun 1996 (8 cruises)	21.75°N	geostrophic (RD = 1000 dbar)	22.9 ± 14.2
<i>Liang et al.</i> [2003]	1991–2000	22–25°N (0–300 m)	Sb-ADCP	15.4–24.3

^aQ, volume transport; RD, reference depth; ETC, East Taiwan Channel; Sb-ADCP, shipboard acoustic Doppler current profilers.

Westward propagation of mesoscale eddies from the interior Pacific Ocean has been frequently attributed to the 100-d variation in the Kuroshio [e.g., *Yang et al.*, 1999; *Zhang et al.*, 2001; *Yang and Liu*, 2003; *Hwang et al.*, 2004].

[5] At the seasonal scales, *Lee et al.* [2001] suggested that transport at PCM-1 is maximum in summer and minimum in fall. *Tang et al.* [2000] and *Liang et al.* [2003], using hydrographic and Sb-ADCP data, showed that the Kuroshio off northeast Taiwan (~25.5°N) is

stronger and farther away from the coast in summer than in winter, a time when the Kuroshio is wider and spreads farther to the shelf area. *Tang et al.* [2000] further suggested that seasonal migration of the Kuroshio axis causes the disappearance of a cyclonic eddy and the associated cold dome off northeast Taiwan. These processes have significant year-to-year variability.

[6] Recent data from numerical models and hydrographic observations have suggested correlation between

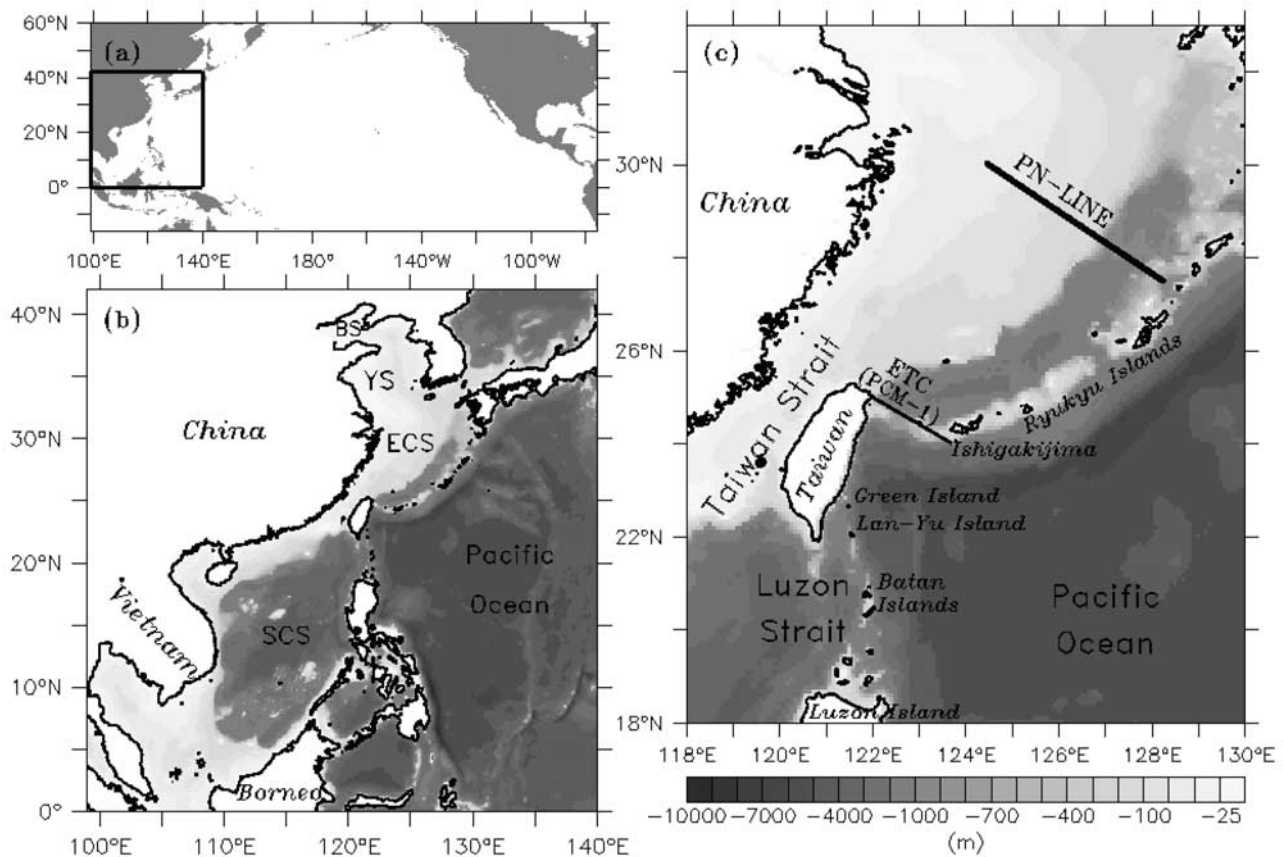


Figure 1. The nested system of numerical simulation. (a) The North Pacific Ocean (NPO) model domain with the East Asian Marginal Seas (EAMS) model domain in a box. (b) The EAMS model domain and bathymetry. (c) Enlarged view of bathymetry in the seas around Taiwan.

the Kuroshio variability and conditions in the source region of the Kuroshio. The transport of the Kuroshio seems to vary with the transport of the North Equatorial Current and the location of its bifurcation point [Qiu and Lukas, 1996; Qu *et al.*, 1998; Kim *et al.*, 2004]. A seasonal maximum in Kuroshio transport usually occurs in the fall (September–October) when the bifurcation point of the North Equatorial Current is northernmost [Qiu and Lukas, 1996; Qu *et al.*, 1998]. Because of the connection between the Kuroshio and the equatorial current system, it is not surprising that variations of the Kuroshio at time-scales of 3–7 years could be traced to those in the North Equatorial Current [Qiu and Lukas, 1996]. For example, the transport southeast of Taiwan was minimum during the 1997–1998 El Niño–Southern Oscillation (ENSO) event and maximum during the non-ENSO periods in 1995 and in 2000 [Gilson and Roemmich, 2002]. Hwang and Kao [2002] calculated the correlation coefficient between the volume transport derived from satellite altimetry and the ENSO sea surface temperature (SST) index. Northeast of Taiwan, the Kuroshio transport variation lags behind the ENSO SST index by a month with a correlation coefficient 0.6. In contrast, the variation in transport southeast of Taiwan leads the ENSO SST index by 9–10 months with a negative coefficient, -0.6 .

[7] The spatial and temporal variability of the Kuroshio east of Taiwan is presumably caused by complicated bathymetry, westward propagating eddies, conditions in the upstream flow, and instability in the Kuroshio. Although short-term current measurements have shed light on these processes, the observational data are limited in both spatial and temporal coverage. Furthermore, year-to-year variations of eventlike mesoscale features are not resolved in earlier modeling studies. In this paper, we have used a nested three-dimensional, primitive equation, numerical ocean model to resolve the key features in observations and to provide a better description of the transport variation than in previous modeling studies.

2. Model Description

[8] The model includes a fine-scale regional model, the East Asian Marginal Seas model (EAMS), nested to a North Pacific Ocean model (NPO). Both component models are three-dimensional with a free surface and solve the equations for momentum, salt concentration, and heat content. The formulation follows that of the sigma coordinate Princeton Ocean Model (POM) [Blumberg and Mellor, 1987]. For example, both models include a two-and-a-half-level turbulence closure submodel developed by Mellor and Yamada [1982] for vertical mixing and the Smagorinsky formulation for horizontal mixing [Oey *et al.*, 1985]. The models also adopt POM's mode-splitting technique, in which the vertically integrated equations for the barotropic (external) mode and the equations for the baroclinic (internal) modes are solved separately. Details of the POM formulation can be found in work by Blumberg and Mellor [1987] and Mellor [2004].

[9] The NPO model covers the North Pacific Ocean from 16°S to 60°N latitude and 99°E to 77°W longitude with a nonuniform resolution in horizontal (Figure 1a). The grid size decreases from 40 km at the equator to 20 km on the

northern boundary. The model has 26 vertical sigma levels. The EAMS model uses realistic bathymetry over an expanded domain including the upstream and downstream regions of the Kuroshio, the South China Sea, and the East China Sea but not the Kuroshio extension region (Figure 1b). The horizontal grid size is $1/8^{\circ}$ in the EAMS model, and there are 26 vertical sigma levels, as in the NPO model. Topography around Taiwan is obtained from the digital bathymetry version-5 model (TaiDBMv5) of the National Center of Ocean Research in Taiwan. The topography is blended with the 5-min elevation data (ETOPO5) of the National Geophysical Data Center [Edwards, 1988].

[10] On open boundaries, the EAMS model derives its values from the NPO model using one-way coupling. From Flather [1976], the vertically averaged normal velocity on the open boundaries of the EAMS model, \bar{u}_n , is derived from the corresponding velocity estimate from the NPO model, \bar{u}_n^0 , using

$$\bar{u}_n = \bar{u}_n^0 + \sqrt{\frac{g}{H}}(\eta - \eta^0), \quad (1)$$

where η is the sea surface height in the EAMS model, η^0 is the NPO model-derived sea surface height, H is the water depth on the open boundary, and g is the gravitational constant. The sea surface height η is located half a grid inside the open boundary in the EAMS model, while η^0 is located on the open boundary of the EAMS model. Baroclinic velocities on the open boundaries of the EAMS model are determined using the inflow scheme by Mellor [2004]: The daily baroclinic velocities from the NPO model are spatially interpolated and assigned to the open lateral boundary grids of the EAMS model. Temperature and salinity on the open boundaries are calculated using an upstream advection scheme [Mellor, 2004]: Daily NPO profiles of temperature and salinity supply the upstream values in case of inflow.

[11] The NPO model is driven by the monthly climatologic wind stress reanalyzed by the National Centers for Environmental Prediction/National Center for Atmospheric Research (NCEP/NCAR) during spin-up. The data set is obtained from the Climate Diagnostics Center of the National Oceanic and Atmospheric Administration (NOAA data are available at <http://www.cdc.noaa.gov/>). After spinning up from rest for 50 years, the model is continuously forced by the NCEP/NCAR reanalysis version 1 wind data from 1948 to 1978 and version 2 wind data from 1979 to 2005. The monthly climatologic SST data derived from NCEP/NCAR reanalysis are used as the surface temperature boundary condition during the spin-up period. The 6-h advanced very high resolution radiometer SST ($2.5^{\circ} \times 2.5^{\circ}$) from NCEP/NCAR is used for the period between 1948 and 1981. From 1982 to 2005, the weekly SST data determined by optimal interpolation with a spatial resolution of $1^{\circ} \times 1^{\circ}$ from the Data Support Section at the Computational and Information Systems Laboratory of NCAR (NCAR data are available at <http://dss.ucar.edu/>) are used.

[12] During spin-up, the EAMS model is initialized by the temperature and salinity fields of the NPO model output in January 1980 and is under climatologic forcing for 2 years.

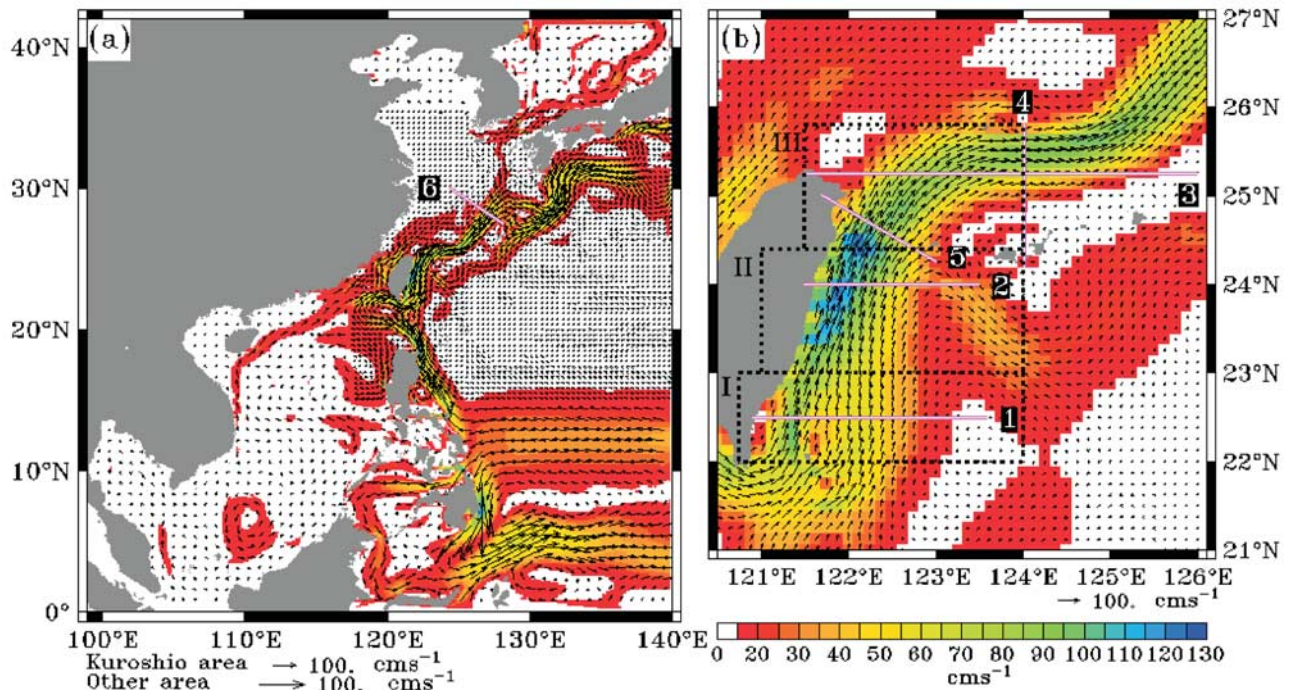


Figure 2. The annual mean surface current averaged from 0 to 50 m (a) in the full EAMS model domain and (b) in the vicinity of Taiwan. The color bar is for both Figures 2a and 2b and represents the current speed. The number of grids is doubled, and the length of the velocity vector is reduced by half from 15 to 35°N and from 120 to 140°E in Figure 2a. Six lines labeled as 1 to 6 indicate the sections for transport calculation at 22.5°N, 24°N, 25.25°N, 124°E, PCM-1, and PN-LINE, respectively.

The EAMS model is then forced by the 6-h NCEP/NCAR reanalysis version 2 wind stress at the sea surface and by the open boundary values provided by the NPO model. The simulation period is from 1980 to 2005. The mean state and variability of the Kuroshio east of Taiwan are investigated using daily model output from the EAMS model between 1982 and 2005, a period when higher spatial resolution SST data are used in the simulation.

3. Result From Model Simulation

3.1. Mean Surface Currents

[13] The annual mean surface current averaged from 0 to 50 m and over 24 years of simulation is plotted in Figure 2a with a close-up view of the Kuroshio east of Taiwan in Figure 2b. Figure 2a is consistent with the classical mean flow pattern in this region [e.g., Nitani, 1972; Centurioni *et al.*, 2004; Zhu *et al.*, 2004]. The Kuroshio originates from the westward North Equatorial Current at 12.5°N. After looping into the Luzon Strait, the Kuroshio flows northward along the east coast of Taiwan and splits into two paths near 24°N. The main path follows the shelf break in the East China Sea. The other turns southeastward along the south edge of the Ryukyu Islands and then northeastward, following the eastern flank of the Ryukyu Islands. The two paths join again south of Japan.

[14] Characteristics of surface currents in Figure 2b can be described in three regions. In region I, the Kuroshio has two high-speed cores, centered at 121.4 and 122°E, respectively. The two cores from region I join in region II, where the Kuroshio is fastest (about 130 cm/s). Branching of the

Kuroshio occurs at the northern edge of region II. The main path of the Kuroshio enters ETC between Taiwan and the Ryukyu Islands, but some water turns southeastward and becomes the offshore branch of the Kuroshio east of the Ryukyu Islands. Note that flow in the southeastward branch would be missed by current measurements along PCM-1. In region III, the Kuroshio turns eastward when encountering the shelf break in the East China Sea.

[15] The flow structure in the Kuroshio is shown in Figure 3 in four vertical sections. In the two southern sections, the northward velocity component V is stronger than the eastward velocity component U . At 22.5°N, the northward velocity has two maxima, consistent with the two-core structure in Figure 2b. The one near the coast is in the upper 300 m with maximum northward velocity (V) over 80 cm/s. The offshore core has a maximum speed of 50 cm/s extending to 600 m. After the two cores join, the Kuroshio at 24°N becomes much deeper and has a single maximum in V velocity near the coast with northward velocity higher than 110 cm/s. The 25.25°N section shows stronger U velocity than V , indicating eastward turning and deepening of the Kuroshio at the shelf break. In the 124°E section, the two cores in eastward velocity with positive U are associated with the two Kuroshio branches, and a strong subsurface countercurrent with negative U is evident between 23 and 24°N. The Kuroshio on the shelf edge in the East China Sea reaches 90 cm/s. The strong subsurface countercurrent has a maximum speed of 40 cm/s at 900 m along the south edge of the Ryukyu Islands. Intrusion of the Kuroshio onto the continental shelf is indicated by weak positive V velocity at the shelf break. The four sections

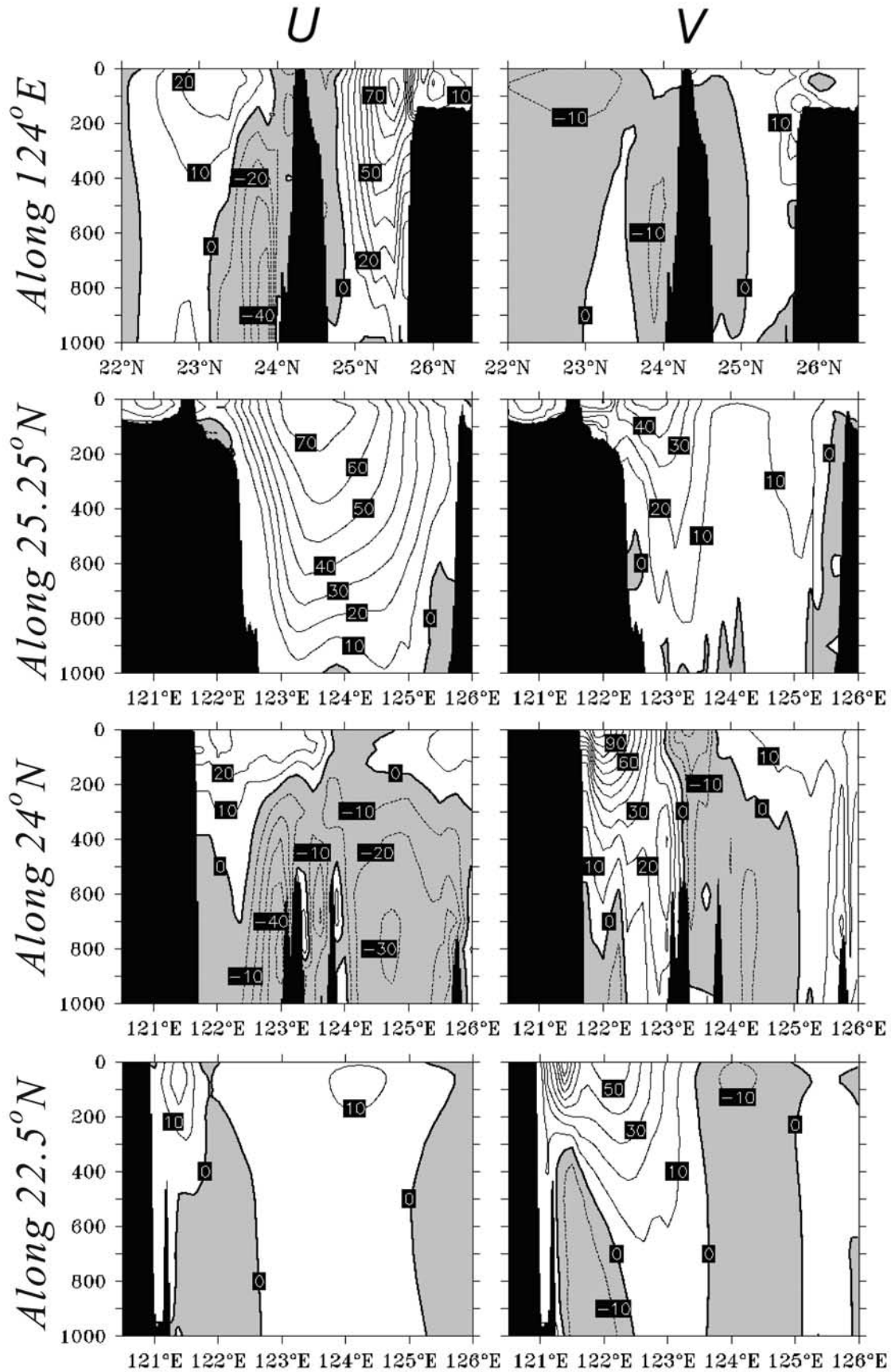


Figure 3

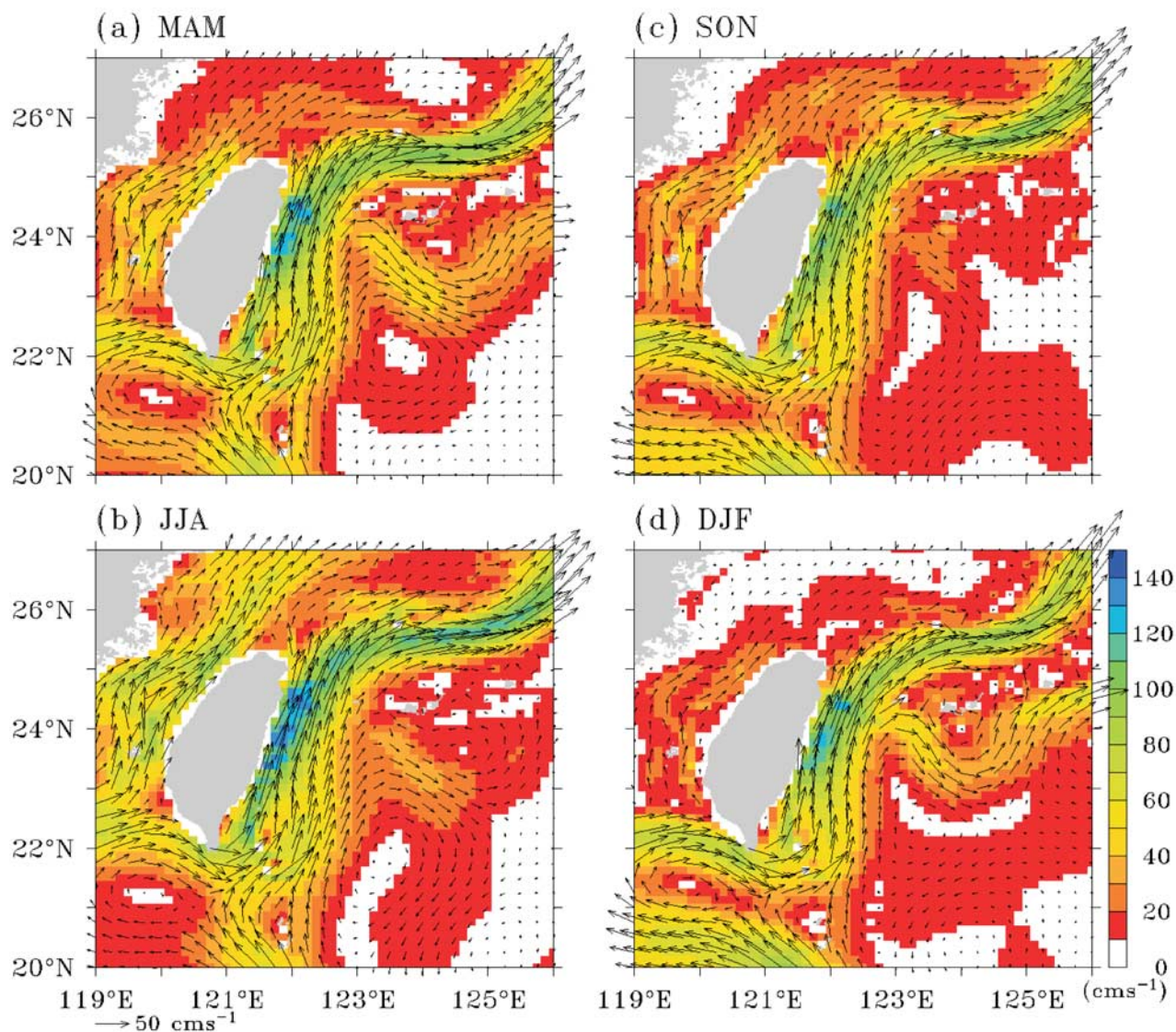


Figure 4. Maximum horizontal currents between 0 and 200 m from model simulation, showing (a) spring, (b) summer, (c) fall, and (d) winter. The unit vector is 50 cm/s, and color-shading indicates current speed.

show deepening of the Kuroshio from 600 m at 22.5°N to 1000 m north of 25.25°N if the 10 cm/s isotach is used to delineate the core of the Kuroshio.

3.2. Seasonal Variation of Currents With Depths

[16] The averaged flow field in each season is studied in three depth ranges. The spring, summer, fall, and winter seasons are defined as March-April-May, June-July-August, September-October-November, and December-January-February, respectively, following the fact that transitions between the winter monsoon and the summer monsoon occur in April and October. Maps of the maximum

velocity between 0 and 200 m depths show the continuous surface path of the Kuroshio in the domain from the southern boundary to the northeast corner (Figure 4). The flow pattern is fairly complicated in the vicinity of the Luzon Strait: a straight path around the Batan Islands and an anticyclonic path into the Luzon Strait. The two paths persist in all seasons, but the relative strength of currents in the two paths varies. The Kuroshio tends to flow in a straight path in spring and summer with weaker flow entering the South China Sea (Figures 4a and 4b). Stronger inflow into the South China Sea occurs in fall and winter when the flow around the Batan Islands is

Figure 3. Vertical distribution of horizontal velocities between 0 and 1000 m in sections at 22.5°N, 24°N, 25.25°N, and 124°E. The velocity is averaged over data from 24-year model simulation. The left panels are zonal velocity component (U), and the right ones are the meridional velocity component (V). The contour interval is 10 cm/s. The negative contours in gray shading denote westward flow in U or southward flow in V .

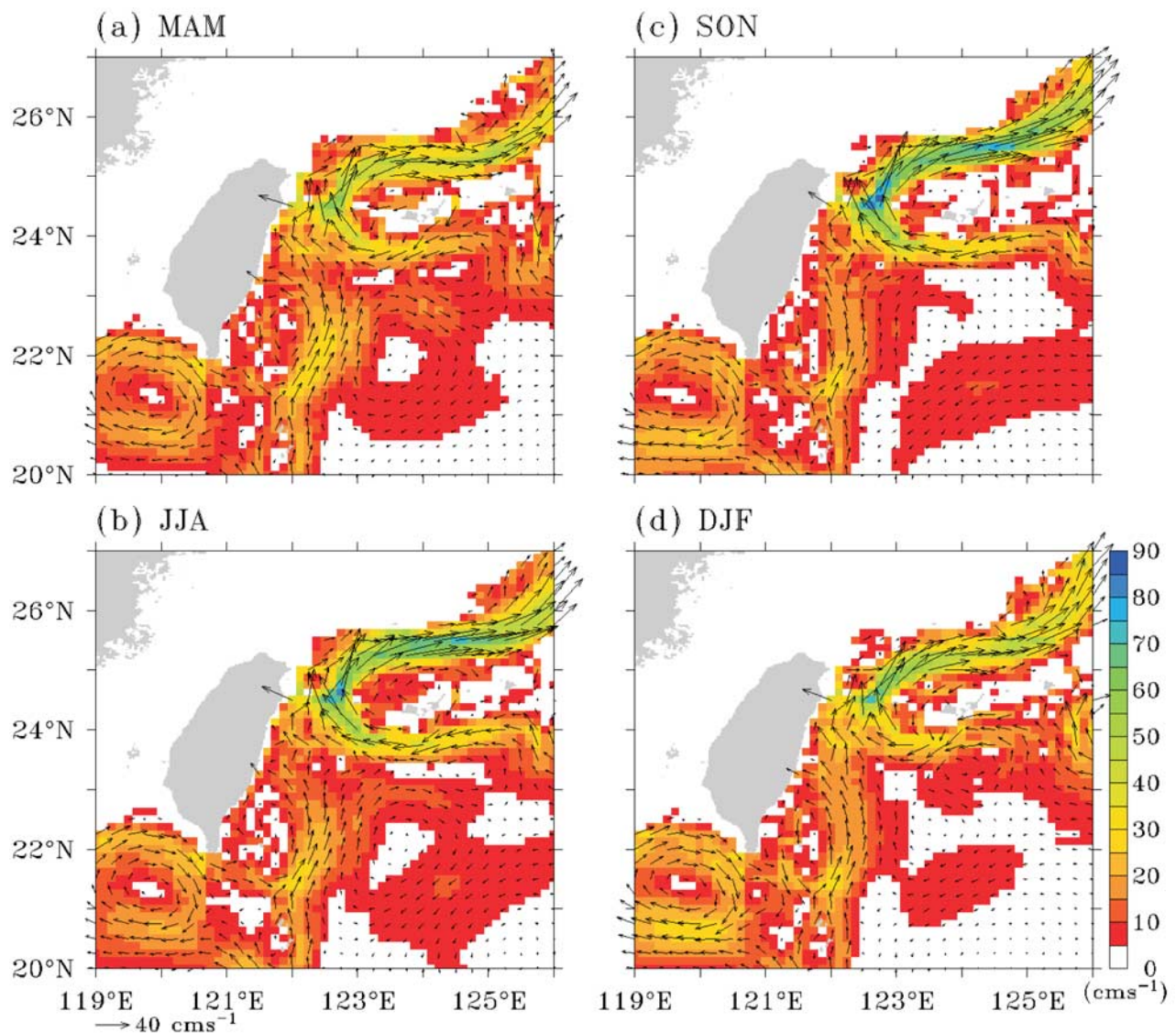


Figure 5. Same as Figure 4 but for flow averaged over 300–600 m. The unit vector is 40 cm/s.

weaker (Figures 4c and 4d). This seasonal dependence agrees with the historical hydrographic observations that intrusion of water from the Kuroshio into the South China Sea occurs mainly in winter [Shaw, 1991]. Contribution of surface water from the South China Sea to the Kuroshio seems to occur around the southern tip of Taiwan, as reported in water mass studies [Gong *et al.*, 1992; Chen and Huang, 1996] and current meter measurements [Liang *et al.*, 2003]. North of Taiwan, some South China Sea water through the Taiwan Strait may also enter the Kuroshio, especially during summer [Chen *et al.*, 1995].

[17] After reaching the coast of Taiwan, the Kuroshio flows in two paths separated by the Lan-Yu Island (Figure 4). This structure is consistent with the two velocity maxima at 22.5°N in Figure 3. The relative strength of currents along the two paths may be associated with the upstream flow at the Batan Islands and the southern tip of Taiwan. At 24°N, the Kuroshio is attached to the coast as the current becomes narrower and stronger. There is slight

seasonal variation in the speed of the Kuroshio, as shown by changes in the blue shading in Figure 4. The speed is slightly higher in summer (~ 140 cm/s) than in fall and winter (~ 120 cm/s). When reaching ETC, the Kuroshio splits on the two sides of the ridge near 24.5°N. The branch north of the ridge enters ETC and forms a strong current on the continental slope in the East China Sea. The branch south of the ridge flows eastward along the south edge of the Ryukyu Islands. In winter and spring, the current is stronger and meanders southward between 123 and 126°E (Figures 4a and 4d). The meander is weaker in summer and almost diminishes in fall (Figures 4b and 4c).

[18] Figure 5 shows maps of vertically averaged velocity between 300 and 600 m in the middle layer of the Kuroshio. The shallow inshore path of the Kuroshio at 22.5°N diminishes in this depth range, consistent with the flow field shown in Figure 3. Only the offshore path appears as an extension of the flow from east of the Batan Islands. The anticyclonic loop into the South China Sea is detached from

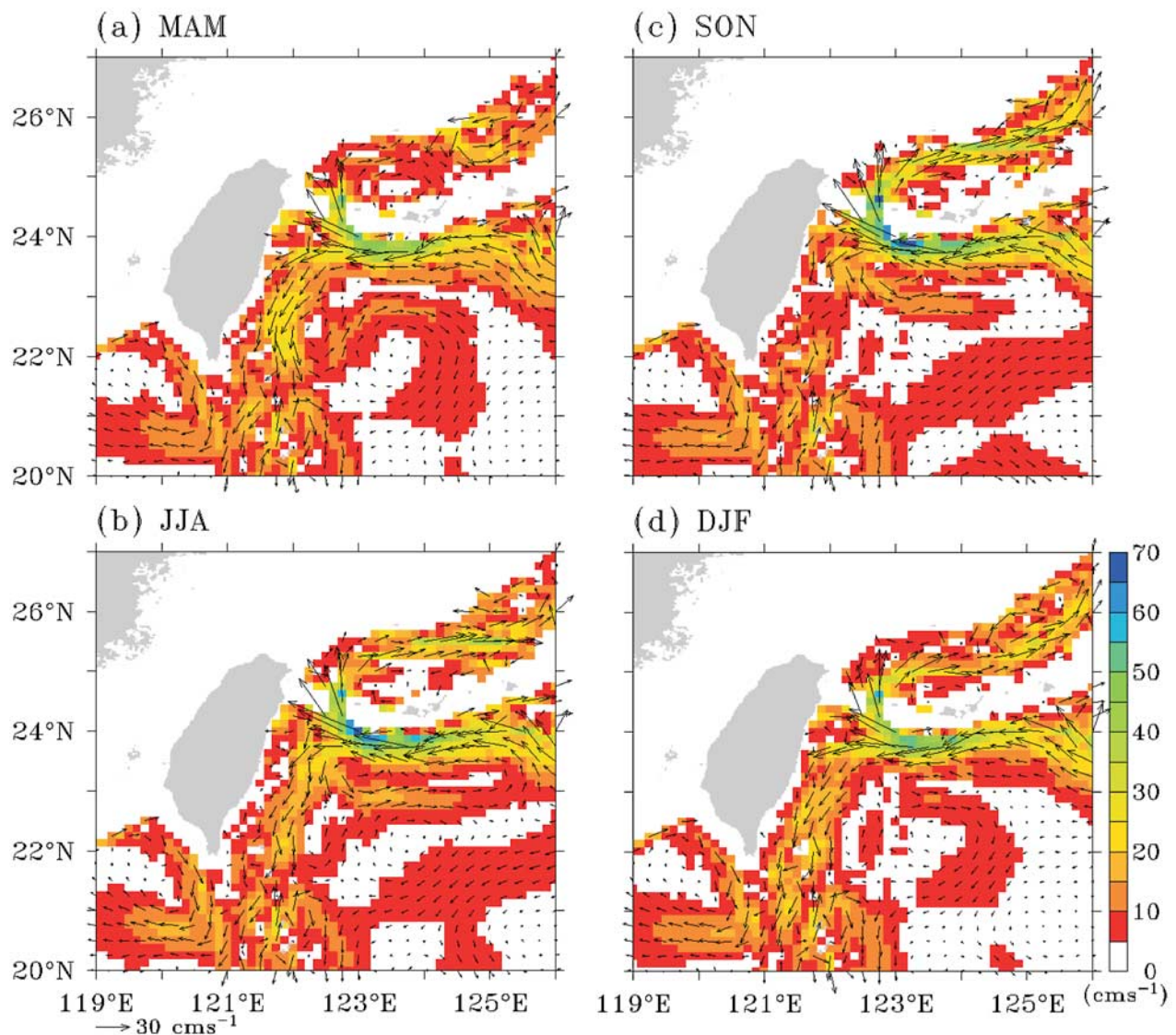


Figure 6. Same as Figure 4 but for flow averaged over 700–1000 m. The unit vector is 30 cm/s.

the Kuroshio, but some exchange of water between the loop and the Kuroshio remains. The Kuroshio turns toward the coast at 24°N and continues into the East China Sea as in the surface current. An anticyclonic gyre centered at 123.5°E, 22°N appears east of the Kuroshio in spring and summer (Figures 5a and 5b) but disappears in fall and winter (Figures 5c and 5d). On the south side of the Ryukyu Islands, a westward flow joins the Kuroshio in the middle layer. Contribution from this westward flow significantly intensifies the eastward flow along the shelf edge in the East China Sea.

[19] Figure 6 shows the depth-averaged velocity between 700 and 1000 m. The westward flow on the south side of the Ryukyu Islands in Figure 5 extends to this depth range and contributes not only to the flow in the East China Sea but also to a southward countercurrent south of 24°N. The contribution to the southward flow is smallest in fall. In spring, flow in the East China Sea is weakest while the southward countercurrent is strongest. In the Luzon Strait,

the anticyclonic circulation in the northern South China Sea persists in this layer.

[20] The instantaneous path of the Kuroshio is further studied in a sequence of snapshots of sea surface height (Figures 7b–7f) and depth-integrated kinetic energy (KE) in the upper 500 m (Figures 7g–7k). The kinetic energy is defined as $\int_{z=0}^{z=500} 1/2 (u^2 + v^2) dz$. The path of the Kuroshio is associated with sharp sea surface height gradients and high KE. The period is from December 1994 to April 1995 when large variation of the Kuroshio transport at PCM-1 took place [Johns *et al.*, 2001; Zhang *et al.*, 2001]. Subsurface ADCP observations [Johns *et al.*, 2001, Figure 7] showed that the transport at PCM-1 is 24 Sv in December 1994, reducing to 16 Sv in late February 1995, and rebounding back to 23 Sv in late March and 27 Sv in late April 1995. The simulated transport at PCM-1 in Figure 7a agrees well with the observed transport variation.

[21] Figure 7 clearly shows the development of the Kuroshio branch south of the Ryukyu Islands. On 1 December, the Kuroshio follows a straight path into the

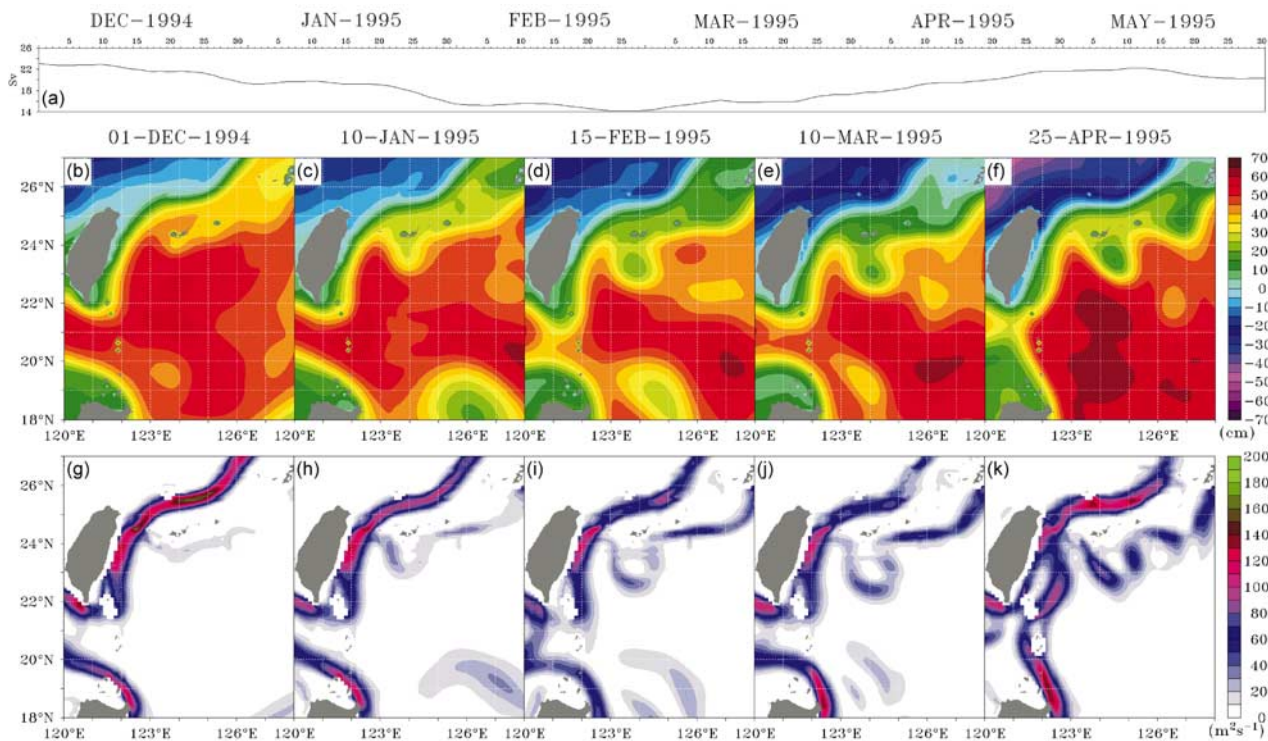


Figure 7. (a) Variation of model-derived transport at PCM-1 from December 1994 to May 1995, (b–f) snapshots of the sea surface height during this period, and (g–k) the kinetic energy in the upper 500 m of the water column.

East China Sea with little energy entering the offshore path (Figure 7b). The KE distribution shows a strong current on the shelf edge and little energy south of the Ryukyu Islands (Figure 7g). The offshore branch of the Kuroshio starts developing on 10 January, as shown in the surface height field (Figure 7c) and in the KE distribution (Figure 7h). Development of the current in the offshore branch is associated with weakening of the flow in the East China Sea, as evidenced by changes in shading from red to blue

in Figures 7i and 7j. On 25 April, the branch of the Kuroshio on the shelf edge strengthens and less energy enters the path south of the Ryukyu Islands (Figure 7k). The change in transport entering the East China Sea at PCM-1 correlates well with the development of the current south of the Ryukyu Islands on the timescale of 3–4 months (Figure 7a).

[22] The sea surface height field shows that the Kuroshio forms a loop in the Luzon Strait on 1 December and 10 January (Figures 7b and 7c). Distribution of KE in the top

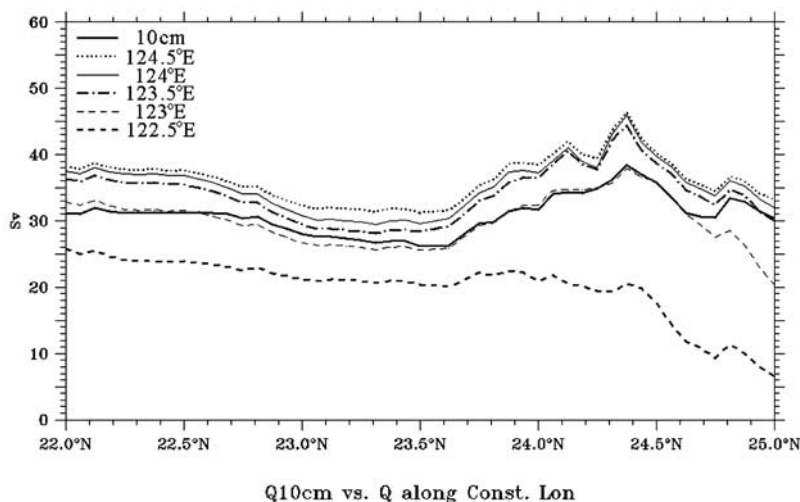


Figure 8. Dependence of the Kuroshio transport on latitude. The thick solid line denotes transport integrated from the coast of Taiwan eastward to the 10 cm/s isotach at the surface. The other lines are transports integrated to five longitude lines: 122.5, 123, 123.5, 124, and 124.5°E.

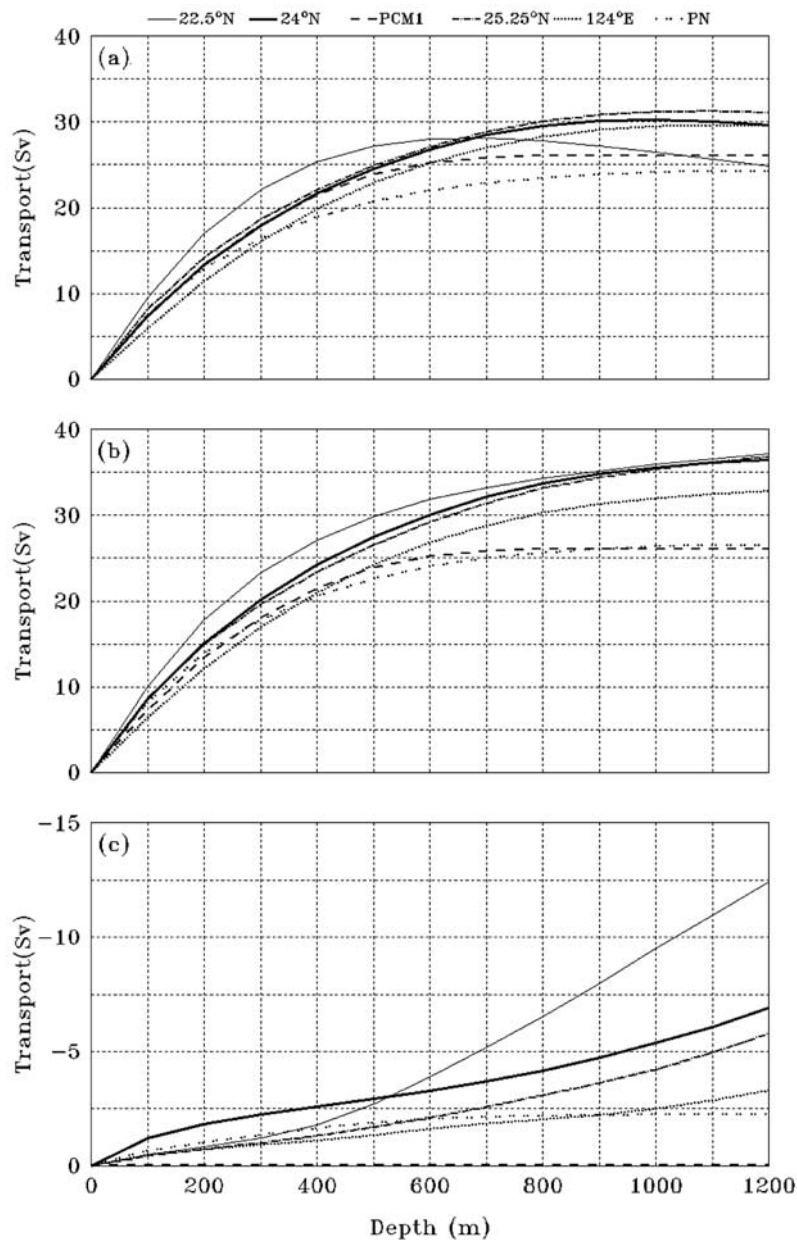


Figure 9. (a) Variation of volume transport as a function of the lower boundary of vertical integration at the six sections shown in Figure 2. Transport is also calculated using flow (b) in the downstream direction only and (c) in the upstream direction only.

500 m of the water column indicates the formation of a loop current (Figures 7g and 7h). After turning around the southern tip of Taiwan, the Kuroshio flows northward along the east coast of Taiwan. On 15 February, the meander in the Luzon Strait may have begun to break off (Figures 7d and 7i). By 25 April, a straight path of the Kuroshio appears east of Luzon and an offshore path off the southeast coast of Taiwan is established (Figures 7f and 7k). This process may affect the transport east of Taiwan.

3.3. Transport

[23] The Kuroshio transport is calculated from the daily velocity field between 0 and 1000 m, using the northward component only, i.e., ignoring the countercurrent. The

transport is then integrated on a zonal section using different criteria for the limit of integration on the east side. The average values over 24 years of simulation from 1982 to 2005 are plotted as a function of latitude between 22 and 25°N in Figure 8. Various lines represent results using different longitudes and the 10-cm/s isotach at the surface as the limit of integration on the open ocean side. The 10-cm/s isotach was used by *Liang et al.* [2003] in their transport calculation. Figure 8 shows that all lines have similar trends and the range is small except that the transport is much lower if the limit of integration is at 122.5°E. Therefore the transport is not sensitive to the integration limit if the integration is extended to a longitude between 123.5 and 124.5°E. Transport shows a minimum at

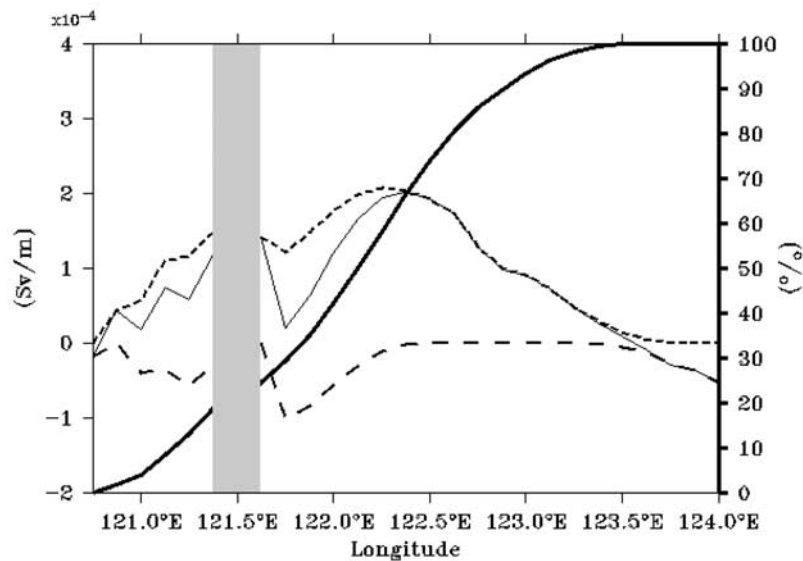


Figure 10. Volume flux at 22°N. (left) Fluxes contributed by the northward and southward flows are shown by short-dashed and long-dashed lines, respectively. The sum of the two is plotted as a thin solid line. (right) The thick solid line is the cumulative percentage of contribution by the northward flow from west. The gray shading indicates the location of the Lan-Yu Island.

23.0–23.5°N and a maximum north of 24°N. The subsurface westward countercurrent south of the Ryukyu Islands increases the transport along the shelf edge north of 24°N (Figure 5). The minimum is likely because of the outflow from the eastern boundary of region I. More detail will be given in section 4.

[24] The average Kuroshio transport between 1982 and 2005 is further calculated at six sections marked as 1 to 6 in Figure 2. Among them, three are zonal sections: 120.9–123.6°E along 22.5°N (section 1), 121.5–123.5°E along 24°N (section 2), and 121.5–126°E along 25.25°N (section 3). Section 4 is along 124°E between 24.2 and 25.8°N. Sections 5 and 6 follow the traditional PCM-1 line in ETC and PN-LINE in the East China Sea, respectively. The transport is integrated from a reference depth of 1000 m to the surface, using the velocity component normal to each section.

[25] The net transport including the countercurrent is plotted in Figure 9a as a function of the lower limit of integration. With the exception of the section at 22.5°N, the transport is not sensitive to the choice of a reference depth between 900 and 1200 m, the range mostly used in the calculation of geostrophic velocity. In fact, the transport at PCM-1 could be accurately estimated using velocity in the top 600 m of the water column. The transport at PN-LINE also changes little if the reference depth exceeds 900 m. However, calculation based on data from Sb-ADCP is often limited to a depth of 300 m and can only capture 65% of the transport. This could explain the lower transport values obtained by *Liang et al.* [2003].

[26] If the countercurrent is excluded from the transport calculation by using only the downstream flow (Figure 9b), transport generally increases with increasing reference depth. The rapid increase in transport of the countercurrent with depth at 22.5°N (Figure 9c) suggests that transport will be overestimated at this section if the reference pressure is

below 600 dbar (Figure 9a). On the other hand, contribution from the countercurrent is insignificant at PCM-1 and PN-LINE. The transport at PN-LINE is 24.1 ± 6.0 Sv, a slight decrease from the upstream transport of 25.8 ± 3.9 Sv at PCM-1. These values are consistent with numbers reported by *Ichikawa and Chaen* [2000] and *Johns et al.* [2001]. Values of the downstream Kuroshio transport above 300 m shown in Figure 9b are 24 Sv at 22.5°N, 20 Sv at 24 and 25.25°N, and 16 Sv at 124°E, respectively. These model-derived values for transport in the upper 300 m are consistent with the observed values given by *Liang et al.* [2003] from composite Sb-ADCP maps between 1990 and 2001 (Table 1).

[27] Variation of the volume flux at 22°N as a function of longitude (Figure 10) shows the transport in the two paths east and west of the Lan-Yu Island (shown by a shaded bar). The northward flux increases toward east, reaching a maximum between 122 and 122.5°E and diminishing beyond 123.5°E in consistency with the assessment earlier. The majority of the transport in the Kuroshio is contributed by the offshore path, which is wider and deeper. The countercurrent reduces the flux east of the Lan-Yu Island but does not change the flux in the core of the offshore path. The cumulative transport integrating eastward shows that about 20% of the Kuroshio transport comes from the path west of the Lan-Yu Island; the rest is in the offshore path.

[28] The 24-year average of the net transport from surface to a reference depth of 1000 m over the five sections exclusive of PN-LINE is 28.4 Sv with a standard deviation of 5.0 Sv (28.4 ± 5.0 Sv). By excluding the countercurrent, the transport increases to 32.7 ± 4.4 Sv. The numbers are comparable to values reported in Table 1, except for the two extremely high values, at 23°N by *Nitani* [1972] and at 24°N by *Liu* [1983]. These measurements were made at latitudes where contribution from the countercurrent is significant. Using a reference depth at 1200 m in the

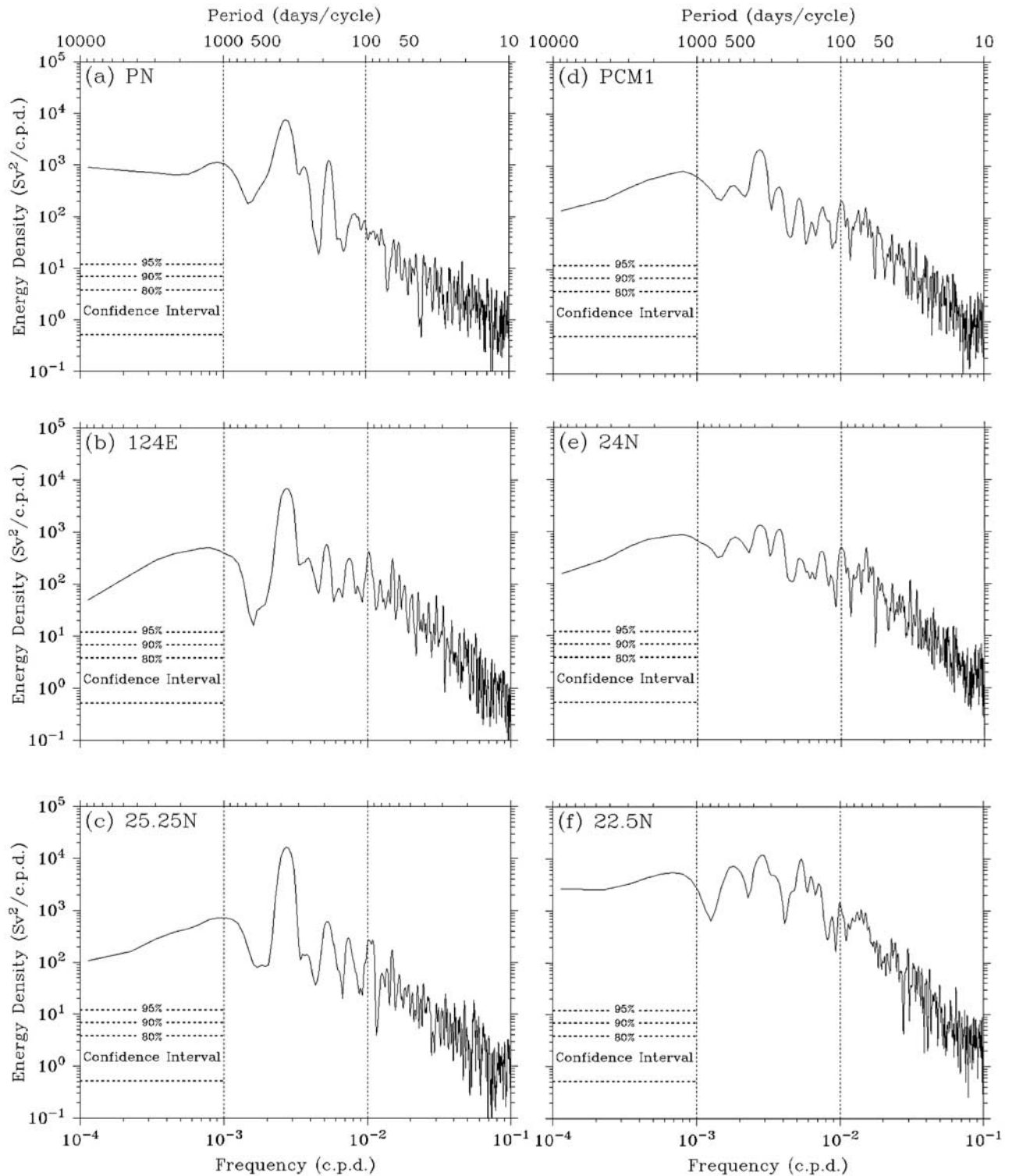


Figure 11. Power spectral density function for downstream transport in Figure 9b. The 80%, 90%, and 95% confidence intervals are shown.

countercurrent as a level of no motion would greatly increase the transport estimate. It is likely that the higher values derived from the model are because of the fact that the velocity field is better resolved in the model simulation than in the observations. The Kuroshio is characterized by fast flow both in the surface layer and near the Taiwan

coast. Limited spatial and temporal coverage of the high-velocity regions tends to underestimate the transport.

[29] Daily transport above 1000-m depth without contribution from the countercurrent is used for calculating the power spectral density function at the six sections (Figure 11). Major peaks at periods of 360 and 180 d are

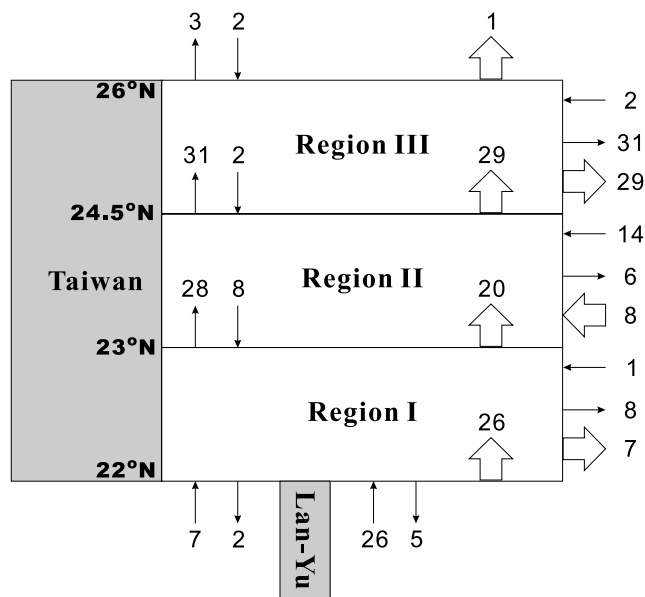


Figure 12. Schematic diagram showing transport in Sv at sections in the Kuroshio east of Taiwan.

mostly in the spectra for northern sections. At sections south of PCM-1, there are also peaks at 2 years and 3–4 years, although both peaks are not significant at the 80% confidence level. In addition to the annual and semiannual cycles, shorter periods between 30 and 180 d are significant except for PN-LINE. High frequency variations between 30 and 70 d may be induced by the

Kuroshio itself or the topographic influence on the current field [Zhang *et al.*, 2001].

4. Discussions

[30] Contributions of the volume transport above 1000 m from the surface flow and countercurrents in three regions east of Taiwan are summarized in Figure 12. Thin arrows indicate flow in and out of a boundary, while thick arrows show the net transport. The number next to an arrow is the transport in Sv. At 22°N, the northward transports are 7 Sv and 26 Sv west and east of the Lan-Yu Island, respectively. The two-path structure of the Kuroshio at 22°N is evident in the trajectories of surface drifters launched during 1988–2004 at a depth of 15 m (Figure 13). The drifters follow two paths represented by solid and dashed lines, respectively. The solid lines are confined in the channel west of the Lan-Yu Island at 121.5°E (the inshore path) and the dashed lines are mainly on the east side of the island (the offshore path).

[31] The net northward flow entering region I is 26 Sv. Most of this water flows northward into region II, but nearly a quarter of the inflow leaves region I from the eastern boundary. The subsurface countercurrent south of Ryukyu Islands flows into region II from east and contributes to both the downstream flow into region III and the southward flow into region I. Most water in region III moves eastward, while a small amount (1 Sv) enters the shelf region.

[32] From current meter measurements at PCM-1, satellite altimeter data, and a numerical model simulation, Zhang *et al.* [2001] suggested that transport of the Kuroshio is affected by meandering of the Kuroshio, which is in turn influenced by westward propagating eddies east of Taiwan,

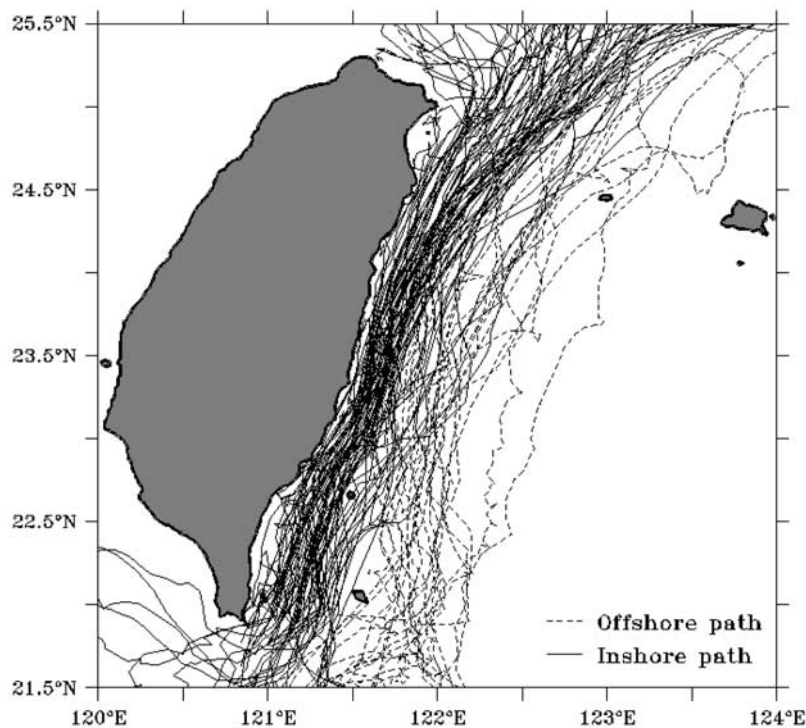


Figure 13. Trajectories of surface drifters passing through the region east of Taiwan from work by Centurioni *et al.* [2004]. The surface drifters were launched at a depth of 15 m during 1988–2004. The solid lines and the dashed lines represent the inshore path and the offshore path, respectively.

southeast of Japan [Ebuchi and Hanawa, 2000], and southeast of the Ryukyu Islands [Zhu et al., 2004]. This process is well demonstrated in Figure 7. During low transport, the Kuroshio bypasses ETC to flow along the east side of the Ryukyu Islands. Yang et al. [1999] proposed that a cyclonic eddy impinging on the Kuroshio near the ridge at 23.5°N reduces the transport and an anticyclonic eddy impinging on ETC increases the transport. The impingement of cyclonic and anticyclonic eddies may be manifestation of the development of a cyclonic meander south of the Ryukyu Islands.

[33] The simulation demonstrates the presence of a strong westward countercurrent below 200 m along the south side of the Ryukyu Islands. A stronger undercurrent may enhance the transport through ETC into the East China Sea (Figure 5). The Kuroshio southeast of Taiwan is also influenced by the countercurrent. The southward flow below 700 m reduces the net northward transport, producing a region of minimum transport between 23 and 23.5°N.

[34] The East China Sea is largely shielded from the open ocean influence by the Ryukyu Islands. The flow inside the island chain is affected by the direction and strength of the East Asian monsoon and shows a strong annual signal, similar to that in the Taiwan Strait [e.g., Chuang, 1986; Wu and Hsin, 2005; Wu et al., 2007] and the South China Sea [e.g., Shaw and Chao, 1994; Wu et al., 1999]. Outside of the Ryukyu Island chain, the flow field east of Taiwan is largely influenced by both cyclonic and anticyclonic eddies with an interval of about 100 d.

5. Conclusions

[35] A fine-scale, three-dimensional, primitive equation, free surface, numerical ocean model has been implemented to investigate the spatial and temporal variations of the Kuroshio east of Taiwan. From 24 years of model simulation, the mean state of the Kuroshio and its deviation from the mean, including the average transport, the structure of the current, and the seasonal variations, are reproduced by the model and are in agreement with observations.

[36] An important finding of this study is that the Kuroshio consists of an inshore path and an offshore path (off southeast Taiwan or at 22°N). The inshore path is likely affected by the water entering the Kuroshio from the loop current around the southern tip of Taiwan, but most transport of the Kuroshio is associated with the deeper offshore path contributed by the flow east of the Lan-Yu Island.

[37] Off northeast Taiwan, the simulation indicates that the surface Kuroshio enters the ETC toward the East China Sea, but a branch may bypass the channel and flow along the south side of the Ryukyu Islands. The branch is mainly in the top 200 m and meanders southward. Transport of the Kuroshio into the East China Sea is reduced when the Kuroshio forms a branch south of the Ryukyu Islands. The transport of the Kuroshio is also affected by a westward subsurface current at 24°N. This current contributes to both downstream Kuroshio transport in the East China Sea and the southward countercurrent east of Taiwan.

[38] The result suggests that transport calculation should choose a reference pressure of 1000 dbar. The modeled downstream transport of the Kuroshio is 32.7 ± 4.4 Sv east of Taiwan. If a shallower depth of 300 m is used, the transport is reduced to 65% of the above value. Spectral analyses of the

transport show that the annual signal is evident east of Taiwan, especially inside the East China Sea. Besides annual signals, energetic peaks are present in the period band from 70 to 170 d, presumably associated with meanders of the Kuroshio and countercurrents east of Taiwan.

[39] **Acknowledgments.** The authors would like to thank L. R. Centurioni for providing the drifter data and the two anonymous reviewers for their careful review of the manuscript and detailed suggestions to improve the manuscript. C.-R. Wu is supported by the National Science Council, Taiwan, under grant NSC 95-2611-M-003-001-MY3, and P.-T. Shaw is supported by the Physical Oceanography Program of Office of Naval Research under contract N00014-05-1-0280.

References

- Blumberg, A. F., G. L. Mellor (1987), A description of a three-dimensional coastal ocean circulation model, in *Three Dimensional Coastal Ocean Models, Coastal Estuarine Stud.*, vol. 4, edited by N. S. Heaps, pp. 1–16, AGU, Washington, D. C.
- Centurioni, L. R., P. P. Niller, and D.-K. Lee (2004), Observations of inflow of Philippine Sea surface water into the South China Sea through the Luzon Strait, *J. Phys. Oceanogr.*, *34*, 113–121.
- Chen, C.-T. A., and M.-H. Huang (1996), A mid-depth front separating the South China Sea water and the Philippine Sea water, *J. Oceanogr.*, *52*, 17–25.
- Chen, C.-T. A., R. Ruo, S. C. Pai, C. L. Liu, and G. T. F. Wang (1995), Exchange of water masses between the East China Sea and the Kuroshio off northeastern Taiwan, *Cont. Shelf Res.*, *15*, 19–39.
- Chu, T.-Y. (1970), Report on the variation of velocity and volume transport of the Kuroshio, in *The Kuroshio: A Symposium on the Japan Current*, pp. 163–174, edited by J. C. Marr, East-West Center Press, Honolulu, Hawaii.
- Chu, T.-Y. (1974), The fluctuations of the Kuroshio current in the eastern sea area of Taiwan, *Acta Oceanogr. Taiwan.*, *4*, 1–12.
- Chu, T.-Y. (1976), Study of the Kuroshio current between Taiwan and Ishigakijima, *Acta Oceanogr. Taiwan.*, *6*, 1–24.
- Chuang, W.-S. (1986), A note on the driving mechanisms of current in the Taiwan Strait, *J. Oceanogr. Soc. Jpn.*, *42*, 355–361.
- Ebuchi, N., and K. Hanawa (2000), Mesoscale eddies observed by TOLEX-ADCP and TOPEX/Poseidon altimeter in the Kuroshio recirculation region south of Japan, *J. Oceanogr.*, *56*, 43–57.
- Edwards, M. (1988), Digital Relief of the Surface of the Earth, *Data Announce. 88-MGG-02*, Mar. Geol. and Geophys., Boulder, Colo.
- Flather, R. A. (1976), A tidal model of the north-west European continental shelf, *Mem. Soc. R. Sci. Liege*, *6*, 141–164.
- Gilson, J., and D. Roemmich (2002), Mean and temporal variability in Kuroshio geostrophic transport south of Taiwan (1993–2001), *J. Oceanogr.*, *58*, 183–195.
- Gong, G.-C., K.-K. Liu, C.-T. Liu, and S.-C. Pai (1992), The chemical hydrography of the South China Sea west of Luzon and a comparison with the west Philippine Sea, *Terr. Atmos. Oceanic Sci.*, *3*, 587–602.
- Hwang, C., and R. Kao (2002), TOPEX/Poseidon-derived space-time variations of the Kuroshio Current: Applications of a gravimetric geoid and wavelet analysis, *Geophys. J. Int.*, *151*, 835–847.
- Hwang, C., C.-R. Wu, and R. Kao (2004), TOPEX/Poseidon observations of mesoscale eddies over the Subtropical Countercurrent: Kinematic characteristics of an anticyclonic eddy and a cyclonic eddy, *J. Geophys. Res.*, *109*, C08013, doi:10.1029/2003JC002026.
- Ichikawa, H., and M. Chaen (2000), Seasonal variation of heat and freshwater transports by the Kuroshio in the East China Sea, *J. Mar. Syst.*, *24*, 119–129.
- Johns, W. E., T. N. Lee, D. Zhang, R. Zantopp, C.-T. Liu, and Y. Yang (2001), The Kuroshio east of Taiwan: Moored transport observations from WOCE PCM-1 array, *J. Phys. Oceanogr.*, *31*, 1031–1053.
- Kim, Y. Y., T. Qu, T. Jensen, T. Miyama, H. Mitsudera, H.-W. Kang, and A. Ishida (2004), Seasonal and interannual variations of the North Equatorial Current bifurcation in a high-resolution OGCM, *J. Geophys. Res.*, *109*, C03040, doi:10.1029/2003JC002013.
- Lee, T. N., W. E. Johns, C.-T. Liu, D. Zhang, R. Zantopp, and Y. Yang (2001), Mean transport and seasonal cycle of the Kuroshio east of Taiwan with comparison to Florida Current, *J. Geophys. Res.*, *106*(C10), 22,143–22,158.
- Liang, W. D., T. Y. Tang, Y. J. Yang, M. T. Ko, and W.-S. Chuang (2003), Upper-ocean currents around Taiwan, *Deep Sea Res., Part II*, *50*, 1085–1105.
- Liu, C. T. (1983), As the Kuroshio turns: (I) Characteristics of the current, *Acta Oceanogr. Taiwan.*, *14*, 88–95.

- Liu, C. T., S. P. Cheng, W. S. Chuang, Y. Yang, T. N. Lee, W. E. Johns, and H. W. Li (1998), Mean structure and transport of Taiwan Current (Kuroshio), *Acta Oceanogr. Taiwan.*, *36*, 159–176.
- Mellor, G. L. (2004), User's guide for a three-dimensional, primitive equation, numerical ocean model, report, 53 pp., Program in Atmos. and Oceanic Sci. Princeton Univ., Princeton, N. J.
- Mellor, G. L., and T. Yamada (1982), Development of a turbulence closure model for geophysical fluid problems, *Rev. Geophys.*, *20*, 851–875.
- Nitani, H. (1972), Beginning of the Kuroshio, in *Kuroshio - Its Physical Aspects*, edited by H. Stommel and K. Yoshida, pp. 129–163, Univ. of Tokyo Press, Tokyo.
- Oey, L. Y., G. L. Mellor, and R. I. Hires (1985), A three-dimensional simulation of the Hudson-Raritan estuary. Part I: Description of the model and model simulations, *J. Phys. Oceanogr.*, *15*, 1676–1692.
- Qiu, B., and R. Lukas (1996), Seasonal and interannual variability of the North Equatorial Current, Mindanao Current, and the Kuroshio along the Pacific western boundary, *J. Geophys. Res.*, *101*(C5), 12,315–12,330.
- Qu, T. (2003), Mixed layer heat balance in the western North Pacific, *J. Geophys. Res.*, *108*(C7), 3242, doi:10.1029/2002JC001536.
- Qu, T., and R. Lukas (2003), The bifurcation of the North Equatorial Current in the Pacific, *J. Phys. Oceanogr.*, *33*, 5–18.
- Qu, T., H. Mitsudera, and T. Yamagata (1998), On the western boundary currents in the Philippine Sea, *J. Geophys. Res.*, *103*(C4), 7537–7548.
- Shaw, P.-T. (1991), The seasonal variation of the intrusion of the Philippine Sea water into the South China Sea, *J. Geophys. Res.*, *96*(C1), 821–827.
- Shaw, P.-T., and S.-Y. Chao (1994), Surface circulation in the South China Sea, *Deep Sea Res., Part I*, *41*, 1663–1683.
- Tang, T. Y., J. H. Tai, and Y. J. Yang (2000), The flow pattern north of Taiwan and migration of the Kuroshio, *Cont. Shelf Res.*, *20*, 349–371.
- Wu, C.-R., and Y.-C. Hsin (2005), Volume transport through the Taiwan Strait: A numerical study, *Terr. Atmos. Oceanic Sci.*, *16*, 377–391.
- Wu, C.-R., P.-T. Shaw, and S.-Y. Chao (1999), Assimilating altimetric data into a South China Sea model, *J. Geophys. Res.*, *104*(C12), 29,987–30,005.
- Wu, C.-R., S.-Y. Chao, and C. Hsu (2007), Transient, seasonal and interannual variability of the Taiwan Strait current, *J. Oceanogr.*, *63*, 821–833.
- Yang, Y., and C.-T. Liu (2003), Uncertainty reduction of estimated geostrophic volume transports with altimeter observations east of Taiwan, *J. Oceanogr.*, *59*, 251–257.
- Yang, Y., C.-T. Liu, J.-H. Hu, and M. Koga (1999), Taiwan current (Kuroshio) and impinging eddies, *J. Oceanogr.*, *55*, 609–617.
- Yaremchuk, M., and T. Qu (2004), Seasonal variability of the large-scale currents near the coast of the Philippines, *J. Phys. Oceanogr.*, *34*, 844–855.
- Zhang, D., T. N. Lee, W. E. Johns, C.-T. Liu, and R. Zantopp (2001), The Kuroshio east of Taiwan: Modes of variability and relationship to interior ocean mesoscale eddies, *J. Phys. Oceanogr.*, *31*, 1054–1074.
- Zhu, X.-H., H. Ichikawa, K. Ichikawa, and K. Takeuchi (2004), Volume transport variability southeast of Okinawa Island estimated from satellite altimeter data, *J. Oceanogr.*, *60*, 953–962.

Y.-C. Hsin and C.-R. Wu, Department of Earth Sciences, National Taiwan Normal University, Number 88, Section 4, Ting-Chou Road, Taipei 11677, Taiwan. (cwu@ntnu.edu.tw)

P.-T. Shaw, Department of Marine, Earth, and Atmospheric Sciences, North Carolina State University, Raleigh, NC 27695-8208, USA.